Current-Loop Control In Switching Converters

Part 5: Refined Model

By Dennis Feucht, Innovatia Laboratories, Cayo, Belize

In the previous sections of this article, we have discussed the historical development of the various models of current-mode control, compared and contrasted those models, and derived various expressions that lay the groundwork for developing a refined version of the unified model originated by Tan and Middlebrook. Here in part 5, we now present a refined model of current-mode control that overcomes some of the limitations of the existing models that have been previously discussed.

A Refined Unified Model

The "unified" models are not fundamentally unified but are piecemeal adaptations of various features of lf-avg and sampled-loop modeling. The phase introduced by sampling does not directly shift $\bar{i}_l$ in the cycle. The constant factor in the PWM transfer function, F_{m0}, is derived from the cycle-averaged inductor current while the dynamics are taken from the sampled-loop model.

For a truly unified model, the full frequency response of the blocks in the block diagram of the model—including static and dynamic factors of transfer functions—should be derived from a single set of general equations describing converter circuits. Tymerski achieved considerable unification of dynamic per-cycle-average inductor current with sampled-loop dynamics in a single set of state-variable equations. Elsewhere, the static F_{m0} was extracted from the discrete-time duty-ratio equations. In Tan and the simple unified model, F_{m0} is extracted out of $\bar{i}_l$ from lf-avg equations but is not used in sampled-loop dynamics derivations.

The direction taken here is to express $\bar{i}_l$ in the discrete time-domain early in the sampling analysis so that subsequent development results in dynamics are based on it, thereby modeling $\bar{i}_l$ dynamically and allowing F_{m0} to fall out of the derivation.

The substitution of $\bar{i}_l$ for i_l in the waveform-derived current-loop transfer function not only changes the constant gain of G_{idV} by ½ but it also introduces additional i_i terms in the difference equation of $\bar{i}_l(k)$ which result in the average-current transfer-function in z:

$$T_C(z)=\frac{\bar{i}_l(z)}{i_i(z)}=\frac{\frac{1}{2}\cdot\left[(D'+1)\cdot z+D\right]}{D'\cdot z+D}=\frac{1}{2}\cdot\left(1+\frac{z}{D'\cdot z+D}\right)=\frac{1}{2}\cdot\left(1+T_{CV}(z)\right).$$

Although the rightmost expression is a simple relationship, it is intractable for further analysis because there is no s-domain transform for the constant (1) term. The $z \rightarrow s^* \rightarrow s$ transform requires $\mathcal{Z}^{-1}\{1\}$, which in the time-domain is a discrete value of 1 at $k = 0$ and is zero elsewhere—an initial value for which there is no defined transform to s. Consequently the expression is retained in the form of the rational function in z.

$T_C(z)$ is transformed to the sampled s-domain;

$$T_C(s)=\frac{\bar{i}_l{}^*(s)}{i_i{}^*(s)}=\frac{\frac{1}{2}\cdot\left[(D'+1)\cdot e^{s\cdot T_s}+D\right]}{D'\cdot e^{s\cdot T_s}+D}.$$

To produce a stepped version of this sampled function, it is multiplied by $H_0(s)$:

$$T_C(s)=\frac{\frac{1}{2}\cdot[(D'+1)\cdot e^{s\cdot T_s}+D]}{D'\cdot e^{s\cdot T_s}+D}\cdot\left(\frac{1-e^{-s\cdot T_s}}{s\cdot T_s}\right)\cdot\frac{e^{s\cdot T_s}}{e^{s\cdot T_s}}=\frac{1}{H_e(s)}\cdot\frac{\frac{1}{2}\cdot[(D'+1)+D\cdot e^{-s\cdot T_s}]}{D'\cdot(e^{s\cdot T_s}-1)+1}=\frac{\frac{1}{2}\cdot[(D'+1)+D\cdot e^{-s\cdot T_s}]}{\left(\frac{s}{\omega_s/2}\right)\cdot\pi\cdot D'+H_e(s)}.$$

Applying Tymerski's two-point fit of $H_e(s)$,

$$H_e(s)\cong\left(\frac{s}{\omega_s/2}\right)^2-\frac{\pi}{2}\cdot\left(\frac{s}{\omega_s/2}\right)+1$$

the resulting approximation is

$$T_C(s)=\frac{\bar{i}_l(s)}{i_i(s)}\cong\frac{1+\frac{D}{2}\cdot(e^{-s\cdot T_s}-1)}{\left(\frac{s}{\omega_s/2}\right)^2+\pi\cdot(\frac{1}{2}-D)\cdot\left(\frac{s}{\omega_s/2}\right)+1}.$$

T_C has the pole-pair of the sampled-loop T_{CV} with stability for $D < ½$. The numerator accounts for the phase shift of $\bar{i}_l(k)$ from the valley value of $i_l(k)$. By applying the two-point "modified Padé" approximation for the exponential,

$$e^{-s\cdot T_s}\cong\frac{\left(\frac{s}{\omega_s/2}\right)^2-\frac{\pi}{2}\cdot\left(\frac{s}{\omega_s/2}\right)+1}{\left(\frac{s}{\omega_s/2}\right)^2+\frac{\pi}{2}\cdot\left(\frac{s}{\omega_s/2}\right)+1}$$

then

$$1+\frac{D}{2}\cdot(e^{-s\cdot T_s}-1)\cong\frac{\left(\frac{s}{\omega_s/2}\right)^2+\frac{\pi}{2}\cdot D'\cdot\left(\frac{s}{\omega_s/2}\right)+1}{\left(\frac{s}{\omega_s/2}\right)^2+\frac{\pi}{2}\cdot\left(\frac{s}{\omega_s/2}\right)+1}.$$

The complete transfer function is

$$T_C(s)=\frac{\bar{i}_l}{i_i}\cong\frac{\left(\frac{s}{\omega_s/2}\right)^2+\left(\frac{\pi}{2}\cdot D'\right)\cdot\left(\frac{s}{\omega_s/2}\right)+1}{\left[\left(\frac{s}{\omega_s/2}\right)^2+\pi\cdot(\frac{1}{2}-D)\cdot\left(\frac{s}{\omega_s/2}\right)+1\right]\cdot\left[\left(\frac{s}{\omega_s/2}\right)^2+\frac{\pi}{2}\cdot\left(\frac{s}{\omega_s/2}\right)+1\right]}.$$

In addition to the sampled-loop pole-pair this function has a pole-pair at a fixed damping of $\zeta = \pi/4 \approx 0.785$ and pole angle of about 38.24°. It also has a LHP complex zero-pair with damping

$$\zeta_z = \frac{\pi}{4} \cdot D'.$$

ζ_z varies with D = [0, ½, 1] by ζ_z = [π/4, π/8, 0] corresponding to zero angles of $\phi_z \approx$ [38.24°, 66.88°, 90°]. The MathCAD plots of T_C are given below with D as parameter, f_s = 200 kHz, L = 100 μH, and V_{off} = 17 V.

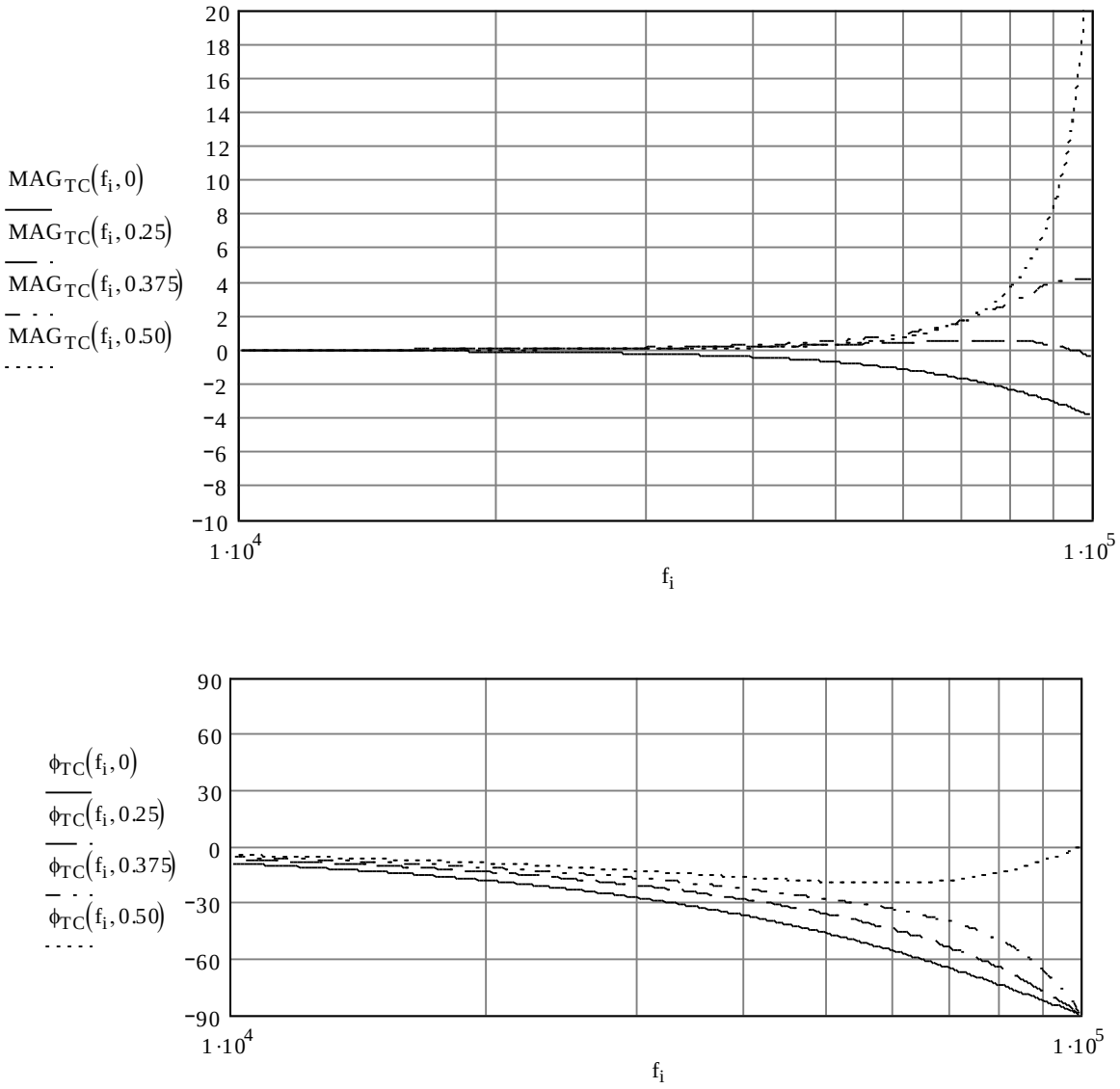

Fig. 1. Average-current transfer-function with D *as parameter.*

$T_C = T_{CV}$ for D = 0, for then either pole-pair and the zero-pair cancel. The zero-pair and both pole-pairs have equal pole radii, that of the Nyquist frequency, $\omega_s/2$. The zero-pair and pole-pair become increasingly underdamped as D increases, moving circularly on the fixed pole radius until they reach the $j\omega$-axis, at D = 1 for the zero-pair and at D = ½ for the pole-pair. As D increases, the pole-pair underdamps more than the zero-pair until it reaches resonance at the Nyquist frequency, where phase is zero. Phase advance of the zero-pair can be seen for T_C near $\omega_s/2$ and D = ½.

Following the construction of the simple unified model, loop sampling is at the error function and a transfer function exists. Equate the expression of $T_C(s)$ with that of the closed feedback loop:

$$T_C(s) = \frac{\bar{i}_l(s)}{i_i(s)} = \frac{F_m(s) \cdot G_{id}}{1 + F_m(s) \cdot G_{id}} = \frac{1}{1 + \dfrac{1}{F_m(s) \cdot G_{id}}}$$

while substituting

$$G_{id}(s) = \frac{\bar{i}_l(s)}{d(s)} = \frac{1}{2} \cdot \frac{i_l(s)}{d(s)} = \frac{V_{off}}{2 \cdot s \cdot L} = \frac{\Delta I_{L0}}{2 \cdot s \cdot T_s} .$$

Then solve for the new expression for $F_m(s)$, which is

$$F_m(s) = \frac{d}{i_{Ce}} = \frac{d}{i_i - \bar{i}_l} = \frac{1}{G_{id}(s) \cdot \left(\dfrac{1}{T_C(s)} - 1 \right)} = \frac{N_C(s)}{G_{id}(s) \cdot \left(D_C(s) - N_C(s) \right)} \; , \; T_C = \frac{N_C}{D_C} .$$

Substituting,

$$F_m(s) \cong \left(\frac{L \cdot \omega_s}{V_{off}} \right) \cdot \frac{\left(\dfrac{s}{\omega_s / 2} \right)^2 + \left(\dfrac{\pi}{2} \cdot D' \right) \cdot \left(\dfrac{s}{\omega_s / 2} \right) + 1}{\left(\dfrac{s}{\omega_s / 2} \right)^3 + \pi \cdot D' \cdot \left(\dfrac{s}{\omega_s / 2} \right)^2 + \left[1 + \left(\dfrac{\pi}{2} \right)^2 \cdot (D' - D) \right] \cdot \left(\dfrac{s}{\omega_s / 2} \right) + \dfrac{\pi \cdot D'}{2}} .$$

In normalized form,

$$F_m(s) \cong \left(\frac{4}{\Delta I_{L0} \cdot D'} \right) \cdot \frac{\left(\dfrac{s}{\omega_s / 2} \right)^2 + \left(\dfrac{\pi}{2} \cdot D' \right) \cdot \left(\dfrac{s}{\omega_s / 2} \right) + 1}{\dfrac{2}{\pi \cdot D'} \cdot \left(\dfrac{s}{\omega_s / 2} \right)^3 + 2 \cdot \left(\dfrac{s}{\omega_s / 2} \right)^2 + \dfrac{2}{\pi \cdot D'} \cdot \left(1 + \dfrac{\pi^2}{2} \cdot (\tfrac{1}{2} - D) \right) \cdot \left(\dfrac{s}{\omega_s / 2} \right) + 1}$$

from which

$$F_{m0} = \frac{4}{D'} \cdot \frac{L \cdot f_s}{V_{off}} = \frac{4}{\Delta I_{L0} \cdot D'} .$$

$F_m(s)/F_m(0\ s^{-1}, D = 0)$ is plotted below in dBV with D as parameter, f_s = 200 kHz, L = 100 µH, and V_{off} = 17 V.

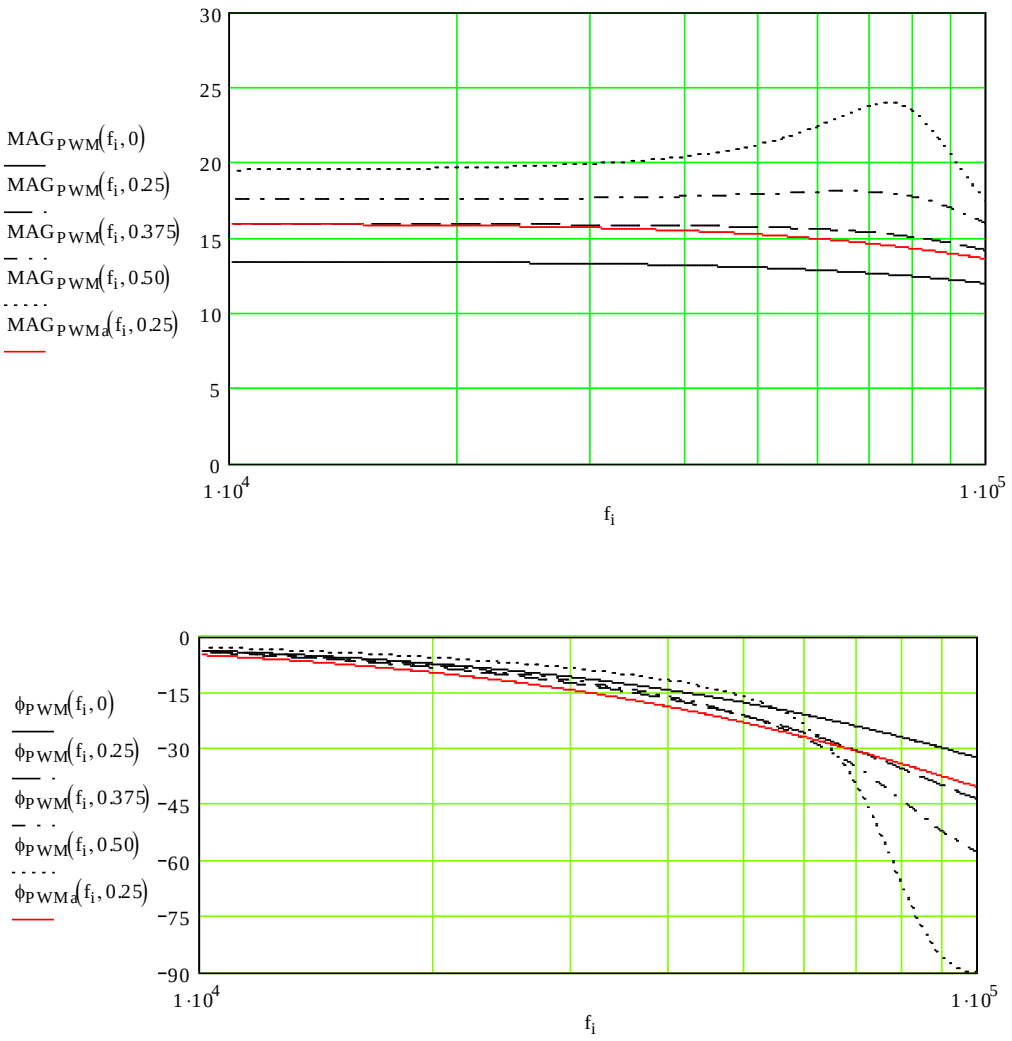

Fig. 2. Normalized PWM transfer function of refined model with D as parameter.

With a G_{id} unity-gain intercept at f_s, then G_{id0} = ½ and for D = ½ the forward-path static gain without slope compensation is one. The forward-path G_0 is twice that of the sampled-loop model. Both magnitude and phase of $F_m(s)$ are flat, increasing significantly in the last decade before the Nyquist frequency. This constitutes a small low-frequency deviation from models that use a frequency-independent F_m, though phase lead in the final decade (approaching 45° for large D) is a significant departure.

The cubic denominator of $F_m(s)$ factors into

$$\left[\left(\frac{s}{\omega_s/2}\right)^2+\frac{\pi}{2}\cdot D'\cdot\left(\frac{s}{\omega_s/2}\right)+1\right]\cdot\left[\frac{2}{\pi\cdot D'}\cdot\left(\frac{s}{\omega_s/2}\right)+1\right]+\frac{-\frac{\pi\cdot D'}{2}\cdot\left(\frac{D}{D'}\right)^2\cdot\left(\frac{s}{\omega_s/2}\right)+1}{\left(\frac{s}{\omega_s/2}\right)^2+\frac{\pi}{2}\cdot D'\cdot\left(\frac{s}{\omega_s/2}\right)+1}$$

where for $[s/(\omega_s/2)]^2 << 1$, then the rightmost term is approximately zero and

$$F_m(s) \cong \left(\frac{4}{\Delta I_{L0} \cdot D'}\right) \cdot \frac{1}{\frac{2}{\pi \cdot D'} \cdot \left(\frac{s}{\omega_s / 2}\right) + 1}.$$

This is not unlike the single-pole $F_m(s)$ of the unified model in Tan. With G_{id} = ½ · G_{idV}, then compared to the sampled-loop static forward-path gain, F_{m0} is effectively $2/\Delta I_{L0} \cdot D'$. This F_{m0} is the same as the Fairchild model.

Unlike the simple-unified model (and that of Tan), at D = ½, F_{m0} does not go to infinity and is

$$F_{m0} = \frac{8}{3} \cdot \frac{1}{\Delta I_{L0}}, D = ½$$

The simple-unified model F_{m0} goes to infinity at D = ½ whereas the alternative F_m expressions remain finite.

$F_m(s)$ does not have the single pole, ω_p, of the simple-unified model. The zero-pair accounts for the phase lead of the average current relative to the valley current at the end of the cycle. The average current leads the valley current sample by $D' \cdot T_s$ and this phase lead is evident in $F_m(s)$ when D is far from zero by the rise in phase in the last decade before the Nyquist frequency. The simple-unified model F_{mV} pole differs by the factor (½ – D) instead of D' when compared to the real pole of the factored denominator of $F_m(s)$ for D = ½. The simple-unified pole of $F_{mV}(s)$ goes to zero at D = ½. As D approaches ½ the responses of the two models diverge. $F_m(s)$ retains the resonance at D = ½ but it does not appear in F_{m0} as it does in F_{mV0}.

In summary, the refined model provides a deeper unification of the quasistatic or low-frequency current-loop behavior with the sampling aspects by deriving the dynamics equations for transfer functions from the average current variable rather than the valley current. The average current extends over the entire switching cycle whereas the valley current pertains to one point in the cycle. This difference results in additional phase shift in the zero-pair of the transfer function of the refined model that accounts for the phase of the average current over the cycle.

What has yet to be considered in the next two sections of this article is the effect of slope compensation, which will be taken up in part 6. Then in the final section, part 7, we will return to a comparison of the important PWM factor, F_{m0} in the current loop and show that the refined model is compatible with the major existing models when reduced to accommodate their limiting assumptions. Finally, what is left to do in completing the current-loop modeling task— that of merging waveform-based and circuit-based modeling—ends this long article.

About The Author

Dennis Feucht has been involved in power electronics for 25 years, designing motor-drives and power converters. He has an instrument background from Tektronix, where he designed test and measurement equipment and did research in Tek Labs. He has lately been doing current-loop converter modeling and converter optimization.

For more on current-mode control methods, see the How2Power Design Guide, select the Advanced Search option, go to Search by Design Guide Category, and select "Control Methods" in the Design Area category.